APL Materials

Temperature-dependent studies of exciton binding energy and phase-transition suppression in (Cs,FA,MA)Pb(I,Br)$_3$ perovskites

Cite as: APL Mater. **7**, 031113 (2019); https://doi.org/10.1063/1.5083792
Submitted: 30 November 2018 . Accepted: 06 March 2019 . Published Online: 26 March 2019

Fabian Ruf, Meltem F. Aygüler, Nadja Giesbrecht, Bettina Rendenbach, Alice Magin, Pablo Docampo, Heinz Kalt, and Michael Hetterich

AIP Publishing

Temperature-dependent studies of exciton binding energy and phase-transition suppression in (Cs,FA,MA)Pb(I,Br)$_3$ perovskites

Cite as: APL Mater. 7, 031113 (2019); doi: 10.1063/1.5083792
Submitted: 30 November 2018 • Accepted: 6 March 2019 •
Published Online: 26 March 2019

Fabian Ruf,[1,a] Meltem F. Aygüler,[2] Nadja Giesbrecht,[2] Bettina Rendenbach,[3] Alice Magin,[1] Pablo Docampo,[4] Heinz Kalt,[1] and Michael Hetterich[1,5,b]

AFFILIATIONS

[1]Institute of Applied Physics, Karlsruhe Institute of Technology (KIT), 76131 Karlsruhe, Germany
[2]Department of Chemistry and Center for NanoScience (CeNS), LMU Munich, 81377 Munich, Germany
[3]Department of Chemistry, LMU Munich, 81377 Munich, Germany
[4]Physics Department, School of Electrical and Electronic Engineering, Newcastle University, Newcastle upon Tyne NE1 7RU, United Kingdom
[5]Light Technology Institute, Karlsruhe Institute of Technology (KIT), 76131 Karlsruhe, Germany

Note: This paper is part of the special topic on Perovskite Semiconductors for Next Generation Optoelectronic Applications.
[a]**Electronic mail:** fabian.ruf@kit.edu.
[b]**Electronic mail:** michael.hetterich@kit.edu.

ABSTRACT

Multiple-cation mixed-halide (Cs,FA,MA)Pb(I,Br)$_3$ perovskites containing cesium, formamidinium (FA), and methylammonium (MA) possess excellent properties for a wide range of optoelectronic applications such as thin-film photovoltaics or lasers. We investigate the role of excitons and the exciton binding energy E_B, relevant for the effectiveness of charge separation in solar cells, as well as the temperature-dependent bandgap energy E_g which is used as an indicator for crystal phase transitions. Generalized Elliott fits of absorption spectra offer the possibility to determine both E_B and E_g. However, since excitonic effects are non-negligible even at room temperature, a careful and detailed analysis of the spectra is crucial for a correct interpretation. Therefore, an additional evaluation based on a so-called f-sum rule is applied to achieve an improved reliability of the results at higher temperatures. The obtained E_B values of 20–24 meV for Cs-containing mixed perovskite compounds are below the ones of 24–32 meV and 36–41 meV for pure methylammonium lead iodide ($MAPbI_3$) and bromide ($MAPbBr_3$), respectively, and, thus, facilitate charge-carrier separation in photovoltaic applications. Furthermore, temperature-dependent (T = 5–300 K) studies of E_g in (Cs,FA,MA)Pb(I,Br)$_3$ indicate a suppressed crystal phase transition by the absence of any phase-transition related signatures such as the well-known jump of about 100 meV in $MAPbI_3$. We verify these results using temperature-dependent electroreflectance spectroscopy, which is a very reliable technique for the direct and non-destructive determination of optical resonances of the absorber layer in complete solar cells. Additionally, we confirm the suppression of the phase transition in $Cs_{0.05}(FA_{0.83}MA_{0.17})_{0.95}Pb(I_{0.83}Br_{0.17})_3$ by temperature-dependent X-ray diffraction.

Organic-inorganic perovskites have demonstrated outstanding optoelectronic properties such as high absorption coefficients,[1] long charge-carrier diffusion lengths,[2,3] and, in particular, an excellent defect tolerance due to high formation energies of deep defects acting as Shockley-Read-Hall recombination centers.[4,5] Because of these characteristics, they are ideal candidates for a broad spectrum of applications ranging from thin-film photovoltaics[6,7] to light-emitting devices[8] including perovskite lasers.[9,10] Starting from methylammonium lead iodide ($MAPbI_3$) as a basic working platform, different material engineering approaches have led to numerous improved compounds containing formamidinium, bromide, and chloride.[11–13] One of the most influential improvements

was the incorporation of cesium into the perovskite crystal structure resulting in an enhanced compositional stability.[14] Moreover, by this approach, the power-conversion efficiency of perovskite solar cells could be further increased to 21.1%,[14] paving the way towards the world record of 23.7% today.[15]

In this contribution, we study the role of excitons and the exciton binding energy E_B as well as crystal phase transitions in these multiple-cation lead mixed-halide perovskites (Cs,FA,MA)Pb(I,Br)$_3$. The formation of excitons can potentially hamper charge separation in solar cells and, therefore, the exciton binding energy is an important indicator in photovoltaics. The occurrence or suppression of phase transitions is crucial also for many other applications in order to maintain a stable performance, e.g., of the solar cell or laser. Since phase-transition related changes of the crystal structure also affect the electronic structure and, thereby, e.g., the bandgap energy E_g, they can be detected using optical spectroscopy.

In this context, absorption spectroscopy is a straightforward measurement technique, and the evaluation by Elliott fits offers the possibility to determine both the exciton binding energy E_B and the bandgap energy E_g.[16,17] However, a careful investigation of the interplay of E_B and E_g is essential for reliable results. Consequently, we present a comprehensive Elliott analysis of absorption spectra of (Cs,FA,MA)Pb(I,Br)$_3$ perovskites to underline their beneficial properties in terms of excitonic effects and suppressed phase transitions.

For our detailed studies, we obtained standard absorption spectra of ~350–450 nm-thick perovskite thin-films on glass from room temperature down to 5 K. Samples were mounted in a liquid helium bath cryostat and illuminated with a halogen lamp. Absorption spectra were obtained using a 0.275 m focal-length monochromator with a 150 lines/mm or 300 lines/mm grating and detected by a charge-coupled device (CCD) camera.

For the evaluation of the measured spectra, we utilized a generalized version of the well-known Elliott formula including spectral broadening Γ of the optical transitions and band non-parabolicity b[16,17]

$$\alpha(\hbar\omega) \propto \frac{1}{\hbar\omega}\left[\underbrace{\sum_j \frac{2E_B}{j^3}\,\mathrm{sech}\left(\frac{\hbar\omega - E_j^B}{\Gamma}\right)}_{\text{Sum of discrete excitonic peaks}} + \underbrace{\int_{E_g}^{\infty} \mathrm{sech}\left(\frac{\hbar\omega - E}{\Gamma}\right)\frac{1}{1-\exp\left(-2\pi\sqrt{\frac{E_B}{E-E_g}}\right)}\cdot\frac{1}{1-\frac{8\,\mu^2 b}{\hbar^4}(E-E_g)}}_{\text{Continuum contribution including Sommerfeld enhancement}}\right], \quad (1)$$

where E_g denotes the bandgap and E_B the exciton binding energy. The term $\frac{\mu^2 b}{\hbar^4}$ (with the reduced electron–hole mass μ) accounts for non-parabolicity in the joint dispersion of valence and conduction band described by $E_C(K) - E_V(K) = E_g + \frac{\hbar^2 k^2}{2\,\mu} - bk^4$. For $b = 0$, the case of perfectly parabolic dispersion is retrieved. The convolution with a bell-shaped function (here a hyperbolic secant function) with width Γ takes spectral linewidth broadening into account.

The first contribution in Eq. (1) consists of a series of excitonic resonances with discrete energy levels $E_j^B = E_g - \frac{E_B}{j^2}$ analogous to the energy levels of the hydrogen atom. The latter summand describes continuum states and accounts for the correlation of electrons and holes due to the Coulomb interaction. This contribution can significantly increase the absorption compared to vanishing excitonic effects and is also known as Sommerfeld enhancement.[18] Figure 1 shows exemplary spectra with Elliott fits (red curve) composed of the sum of discrete excitonic peaks (blue curve) and continuum states (green curve) at T = 20 K for methylammonium lead bromide ($MAPbBr_3$) and two different compounds of Cs-containing mixed perovskites: $Cs_{0.05}(FA_{0.83}MA_{0.17})_{0.95}Pb(I_{0.83}Br_{0.17})_3$ (abbreviated as Cs0.05) and $Cs_{0.1}FA_{0.765}MA_{0.135}Pb(I_{0.765}Br_{0.235})_3$ (Cs0.10). As clearly visible from these spectra [and Eq. (1)], the Elliott fit is based on the interplay of the excition binding energy E_B and the bandgap energy E_g since the energy of the excitonic peak is below E_g by E_B. Therefore, a reliable determination of the bandgap energy E_g also requires an understanding of E_B, since excitonic effects play a significant role for the interpretation of the absorption spectra even at room temperature [illustrated in Fig. 2(b)].

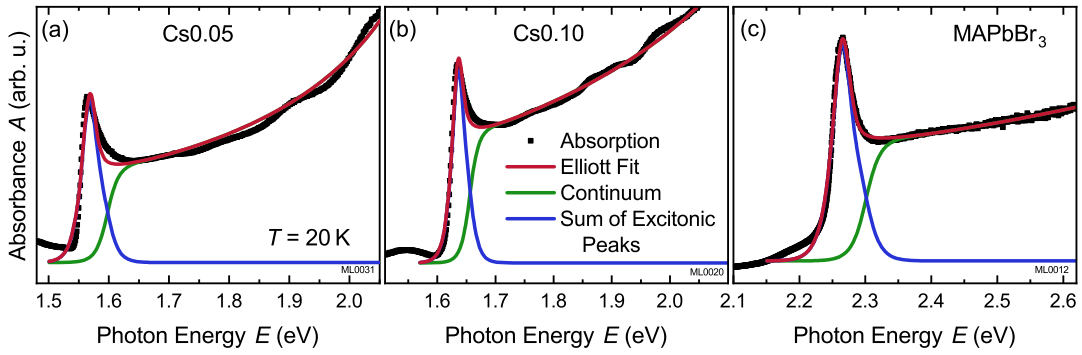

FIG. 1. Exemplary spectra with Elliott fits (red curves) consisting of discrete excitonic peaks (blue curves) and continuum contribution (green curves) of (a) $Cs_{0.05}(FA_{0.83}MA_{0.17})_{0.95}Pb(I_{0.83}Br_{0.17})_3$ (Cs0.05), (b) $Cs_{0.1}FA_{0.765}MA_{0.135}Pb(I_{0.765}Br_{0.235})_3$ (Cs0.10), and (c) $MAPbBr_3$ at T = 20 K.

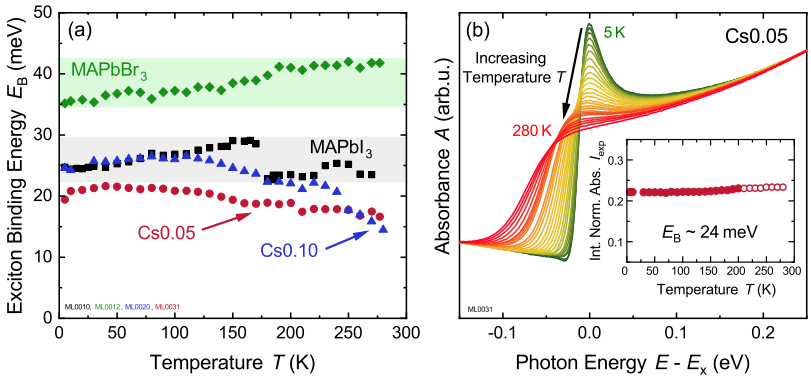

FIG. 2. (a) Estimates for the exciton binding energy E_B of pure $MAPbI_3$ (black squares) and $MAPbBr_3$ (green diamonds) as well as Cs0.05 (red circles) and Cs0.10 (blue triangles) mixed perovskites acquired by Elliott fits to the measured absorption spectra (corresponding to spectra as in Fig. 1). For $MAPbI_3$, the phase transition is visible around T = 160 K. Cs0.05 and Cs0.10 exhibit smaller values for E_B even compared to $MAPbI_3$. However, the accuracy of these values might be compromised at higher temperatures. (b) Normalized absorption spectra shifted by the energy position E_x of the excitonic peak. The spectra are integrated over the whole depicted energy range to determine E_B by using the "absorption f-sum rule". Inset: Integrated normalized absorbance I_{exp}, which is essentially constant, as expected from theory (open circles denote values determined from spectra for which E_x was linearly extrapolated). By "inverting" $I(E_B)$, the exciton binding energy can be determined.

In order to study the exciton binding energy in these multiple-cation mixed-halide perovskites in detail, we extracted the values for E_B from Elliott fits to the measured absorption spectra. (We estimate the accuracy of E_B to be around 5 meV.) The results are summarized in Fig. 2(a) (corresponding to spectra as in Fig. 1). As previously reported, e.g., by Sestu *et al.*,[19] we can confirm a slightly smaller exciton binding energy for the high-temperature tetragonal phase compared to the low-temperature orthorhombic phase for $MAPbI_3$ as well as a much larger E_B for $MAPbBr_3$. Compared to their values of 34 meV and 29 meV for the orthorhombic and tetragonal phase, respectively, in $MAPbI_3$ and 60 meV for $MAPbBr_3$, we found smaller values of E_B = 22–29 meV for $MAPbI_3$ (black squares) and E_B = 35–42 meV for $MAPbBr_3$ (green diamonds), respectively.

Especially for $MAPbI_3$, our values are comparable to other reports using similar optical spectroscopy, e.g., by Saba *et al.* (25 meV)[17] or Sestu *et al.*[19] Still, also lower results around 10 meV or below for E_B have been determined by other techniques such as magnetoabsorption spectroscopy.[20,21] However, even for values in the order of thermal energies at room temperature, calculations of the ratio between free charges and excitons by D'Innocenzo *et al.*[22] and Saba *et al.*[17] show that efficient charge collection is possible under photovoltaic-relevant illumination intensities at room temperature.

More importantly, we clearly observe an overall trend to even lower exciton binding energies for the Cs-containing perovskite compounds ranging from E_B = 16–21 meV for Cs0.05 (red circles) and E_B = 14–26 meV for Cs0.10 (blue triangles), respectively, compared to those for pure $MAPbI_3$ and $MAPbBr_3$. The incorporation of FA might lead to slightly lower values for E_B as has been reported for pure $FAPbI_3$ compared to $MAPbI_3$, e.g., by magnetoabsorption measurements (14 meV compared to 16 meV at cryogenic temperatures and 10 meV compared to 12 meV at around 160 K).[21] On the other hand, we found increased values of 26–31 meV for $MAPb(I_{0.75}Br_{0.25})_3$ compared to $MAPbI_3$.

In any case, the reduced exciton binding energies of Cs-containing mixed perovskites emphasizes their beneficial properties for photovoltaics due to the even higher ratio of free charge carriers and, thus, more efficient charge separation and collection.

However, as the discrete excitonic peak cannot be reliably resolved for increasing temperatures due to increasing linewidth broadening Γ [illustrated in Fig. 2(b) for Cs0.05, green to red curves], the accuracy of the determination of E_B at higher temperatures is compromised. In principle, this also holds for the bandgap energy E_g but it is much less critical because E_g is much larger than E_B leading to only minor deviations. Since the interplay of Γ and E_B determines how pronounced the discrete excitonic peak shows up in the spectrum, this issue gets more critical for compounds with smaller exciton binding energies E_B which could explain the rather unstable values of Cs0.05 and Cs0.10.

In order to account for this effect, Sestu *et al.* developed a so-called "absorption f-sum rule" to facilitate a more precise determination of E_B especially in the case of small E_B and high Γ.[19] It is based on the fact that the oscillator strength of an optical transition (as well as the slope of the continuum contribution) is unaffected by the spectral broadening Γ. Therefore, the integrated normalized absorption I of the excitonic peak (and a certain part of the continuum) becomes a function which only depends on E_B and the non-parabolicity factor $\frac{\mu^2 b}{\hbar^4}$. Since $\frac{\mu^2 b}{\hbar^4}$ is expected to stay approximately constant and can be determined at lower temperatures, the integrated normalized absorption I can be used as a measure for the exciton binding energy. In fact, the sensitivity of the method is influenced by the choice of the integration limits because it determines the ratio of the discrete and continuum contribution which shows a different dependency on E_B. A detailed and illustrated discussion of the theoretical background and practical application of this method can be found in Ref. 19.

Figure 2(b) shows the absorption spectra of Cs0.05 for T = 5–280 K (green to red curves) which were shifted by the energy position of the excitonic peak E_x. (For the spectra T = 210 K and above, E_x could not be determined precisely and was extrapolated linearly.) The spectra were integrated over the whole depicted energy range from −0.15 eV up to E_n = 0.25 eV. E_n also serves as

TABLE I. Summary of the obtained exciton binding energies E_B either directly taken from Fig. 2 (first two rows) or by utilizing the so-called "absorption f-sum rule" method for temperatures above 150 K (last row).

	Exciton Binding Energy E_B (meV)			
Temperatures (K)	Cs0.05	Cs0.10	$MAPbI_3$	$MAPbBr_3$
10	21	24	24	36
150	19	25	29	38
>150	24	20	32	41

normalization energy of the absorption. The resulting integrated normalized absorption I is depicted in the inset of Fig. 2(b) and remains nearly constant as expected from theory. By normalization and numerical integration from −0.15 eV to 0.25 eV of Eq. (1) (for a known non-parabolicity factor $\frac{\mu^2 b}{\hbar^4}$), the resulting $I_{\mathrm{calc}}(E_B)$ can be used to map the measured $I_{\mathrm{exp}}(E_B)$ in order to obtain absolute values for E_B. Since we are interested in values for E_B at high temperatures up to room temperature, we restricted the temperature range of the considered values for I and $\frac{\mu^2 b}{\hbar^4}$ to be above 150 K. For Cs0.05, this "inversion" of $I(E_B)$ yields an exciton binding energy $E_B = 24$ meV, where we estimate the accuracy of the obtained values to be in the range of 5 meV.

Table I summarizes the obtained exciton binding energies E_B for the different investigated compounds. The first two rows show the values which are directly taken from Fig. 2(a), whereas the last row presents the results obtained by the f-sum rule for temperatures above 150 K. The values of the f-sum method and the direct fitting of the Elliott formula match quite well with mainly slightly higher E_B for the f-sum determination, e.g., for $MAPbI_3$ and $MAPbBr_3$. However, especially for the low-E_B Cs compounds, the f-sum method can be expected to yield more reliable results. From this evaluation, we can state that the exciton binding energy E_B of Cs0.05 and Cs0.10 is even lower than for pure $MAPbI_3$ also for temperatures approaching room temperature. This emphasizes the excellent suitability of multiple-cation mixed-halide perovskites for photovoltaics since smaller exciton binding energies are beneficial for the charge separation and, therefore, the charge extraction in the device, as discussed above.

Since the exciton binding energies E_B are only weakly dependent on temperature (as determined by Elliott fits and f-sum rule method), we can analyze the bandgap E_g for temperatures from $T = 5$ K up to room temperature which were extracted from the Elliott fits (see Fig. 1). The results are depicted in Figs. 3(a) and 3(b) together with phase transition temperatures for methylammonium lead bromide and iodide from the report of Poglitsch and Weber.[25] For $MAPbI_3$ [black squares, Fig. 3(b)], we observed the well-known distinct jump in bandgap energy E_g of about 100 meV at the phase transition from the low-temperature orthorhombic to the tetragonal phase around $T_p = 162$ K.[22,26] However, the exact temperature for the bandgap jump can be shifted towards higher or lower values depending on the measurement direction. This "temperature hysteresis" effect is caused by the spatially non-uniform process where some domains still maintain their crystal phase even beyond the phase transition temperature.[27]

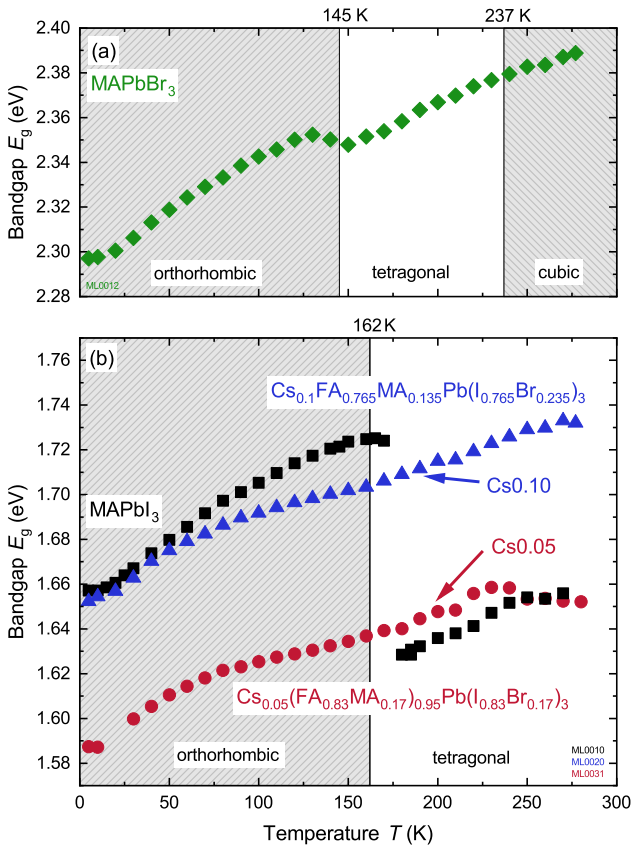

FIG. 3. Bandgap energies E_g of different perovskite thin films determined from generalized Elliott fits to absorption spectra from $T = 5$ K up to room temperature (corresponding to the results in Fig. 2). (a) For $MAPbBr_3$, the phase transition from the low-temperature orthorhombic phase to the tetragonal phase is visible as a kink in the bandgap energy. (b) $MAPbI_3$ (black squares) exhibits clearly the well-known phase-transition related jump of around 100 meV in bandgap energy. Both Cs-containing perovskite compounds (red circles and blue triangles) do not show any phase-transition related features.

For $MAPbBr_3$, we found that the orthorhombic to tetragonal phase transition is visible in the absorption data as well, not as a clear jump, but rather as a small kink [Fig. 3(a)]. Interestingly, Dar *et al.* did not observe such a phase-transition related feature in their photoluminescence measurements for $MAPbBr_3$, but for formamidinium lead bromide instead.[28] The kink might be caused by the co-existence of MA-ordered and MA-disordered domains with different bandgap energies as proposed by theoretical calculations.[28]

Building on these reference measurements for pure $MAPbI_3$ and $MAPbBr_3$, we looked for similar features for the Cs0.05 and Cs0.10 compounds. Mainly due to the higher content of Cs and bromide, the Cs0.10 perovskite exhibits an overall higher bandgap energy.[11,29] However, the temperature-dependent bandgap energy of both compounds does not show any phase-transition related jumps or kinks as in the pure $MAPbI_3$ or $MAPbBr_3$ case [Figs. 3 and 4(b)]. This is a first indication of the suppression of the phase transition in these multiple-cation mixed-halide perovskites.

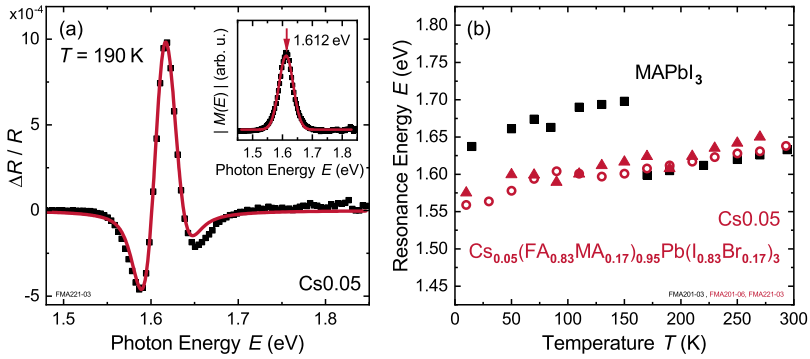

FIG. 4. (a) A typical ER spectrum at T = 190 K. The characteristic feature at the optical resonance can be fitted using a FDFF line shape. Inset: For the determination of the resonance energy, the measured $\Delta R/R$ spectra can be transformed to a so-called modulus spectrum $|M(E)|$ which enables a facile determination of the resonance energy from the energy position of the maximum.[23,24] (b) Optical resonance energies of $MAPbI_3$ (black squares) and Cs0.05 (red symbols, triangles and circles denote different samples) for temperatures from T = 5 K up to room temperature. For $MAPbI_3$, the clear jump in the resonance energy around $T_p \approx 160$ K is related to the orthorhombic-to-tetragonal phase transition as seen in the absorption data in Fig. 3. The absence of a similar feature in Cs0.05 indicates the suppression of possible phase transitions. Data partly shown in Ref. 18.

In order to further support these conclusions, we performed temperature-dependent electroreflectance (ER) spectroscopy measurements for the determination of the optical transition energies.[30,31] In comparison to the presented analysis of absorption spectra, ER spectroscopy provides a very sensitive and robust experimental technique mainly independent of many setup parameters and further theoretical assumptions.[23,24,31] Furthermore, it can be non-destructively applied to complete and non-transparent solar cells in order to probe the absorber in the real device with additional charge-extraction layers and metal back contact.[32–35]

Since this technique belongs to the group of modulation spectroscopy, the fundamental principle is to measure the response of the absorber to an external modulation. In the case of ER spectroscopy, this is realized by applying an AC bias to periodically modulate the electric field in the absorber layer which, in turn, modulates the dielectric function ε. The change $\Delta\varepsilon$ can be experimentally detected by the change of related optical properties: in this case, the change ΔR of the reflectance R. By recording the relative change $\Delta R/R$, the spectra are independent of setup characteristics such as lamp spectrum or detector's spectral response. For the ER measurements, we integrated $MAPbI_3$ and Cs0.05 absorber layers into a commonly used layer stack consisting of FTO[36]/TiO_2/perovskite/spiro-OMeTAD[37]/gold.

Figure 4(a) shows an exemplary ER spectrum with the characteristic resonance feature at the optical transition energy which can be obtained by fitting suitable line shapes to the experimental data. For excitonic systems, a so-called "First-Derivative Functional Form" (FDFF)[38–40] is the appropriate choice which reproduces the measured data nicely as can be seen in Fig. 4(a). Further details about other fitting methods and theoretical line shapes can be found in Refs. 34, 41, and 42.

If only a reliable determination of the energy position of the resonance is of interest, independent of any specific theoretical line shape assumptions, a transformation method based on Kramers–Kronig relations can be utilized.[23,24] The measured $\Delta R/R$ is considered as real part of a complex quantity $M(E)$. By applying Kramers–Kronig relations, the imaginary part and, thereby, the modulus $|M(E)|$ of $M(E)$ can be calculated. This so-called modulus spectrum $|M(E)|$ exhibits a peak-like line shape as illustrated in the inset of Fig. 4(a). The resonance energy then corresponds to the energy position of the maximum which is independent of any theoretical line shape considerations and can be accurately determined. For semiconductors with pronounced excitonic properties such as organic-inorganic perovskites, the resonance energy is not identical to the bandgap, but rather to the discrete excitonic transitions corresponding to the blue curves in Fig. 1. Further details can be found in Ref. 18.

We performed temperature-dependent ER measurements from 5 K up to room temperature. The obtained resonance energies for $MAPbI_3$ and Cs0.05 are depicted in Fig. 4(b). Similar to the bandgap behavior in Fig. 3(b), the resonance energy for $MAPbI_3$ (black

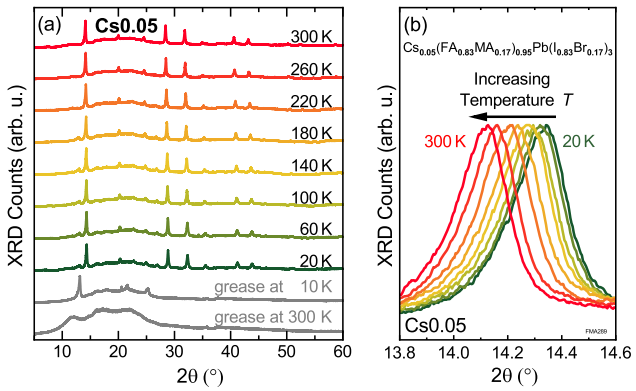

FIG. 5. (a) Temperature-dependent X-ray powder diffraction patterns for Cs0.05 from T = 10–300 K. Despite the expected shifts due to lattice expansion [see (b)], no phase-transition related changes in the diffraction patterns are visible, confirming the suppression of possible phase transitions. (b) Enlargement for the perovskite peak around 14.2°. As expected, the reflection shifts towards smaller diffraction angles with increasing temperature due to lattice expansion.

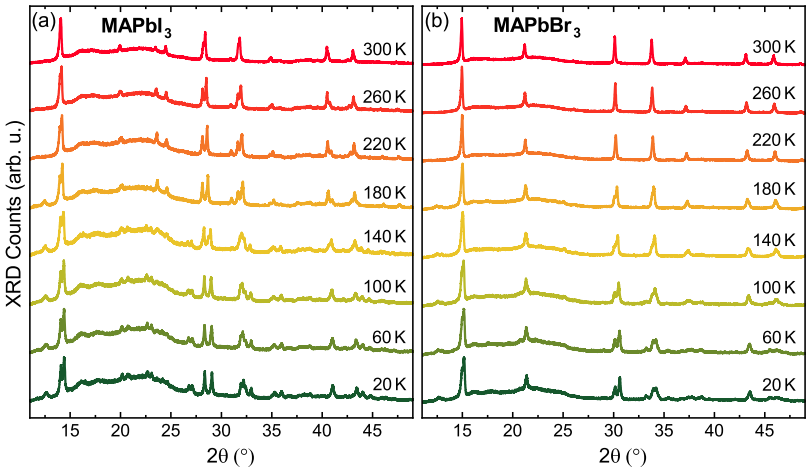

FIG. 6. Temperature-dependent X-ray powder diffraction patterns for (a) $MAPbI_3$ and (b) $MAPbBr_3$ from T = 20–300 K. The changes in the diffractograms clearly indicate a phase transition in both perovskite compounds.

squares) exhibits a clearly visible jump of about 100 meV around the phase transition temperature of $T_p \approx 160$ K from the orthorhombic to the tetragonal crystal phase. In comparison to this, the resonance energy of Cs0.05 (red symbols, triangles, and circles denote different samples) does not show any similar phase-transition related jump. Since ER spectroscopy directly and reliably yields the optical resonance energies in complete devices, we conclude that the orthorhombic-to-tetragonal phase transition is suppressed not only in thin-films on glass but also in complete Cs-containing multiple-cation perovskite solar cells. This might be also relevant for other types of applications such as lasers based on mixed perovskites.

In order to confirm our spectroscopic results suggesting a suppressed phase transition in Cs0.05 also by structural characterization, we performed temperature-dependent X-ray powder diffraction measurements in the range of 10–300 K.

The results are summarized in Fig. 5 (green to red curves for increasing temperature). The patterns of the grease necessary for the measurements are plotted for comparison and can account, e.g., for the contribution around 13°. Figure 5(b) shows a shift of the perovskite reflex at around 14.2°. With increasing temperature, the perovskite crystal lattice expands, resulting in a shift to lower diffraction angles of the corresponding reflexes. Despite the expected change in perovskite crystal lattice size, no phase-transition related change of the X-ray diffractogram was observed, as can be clearly seen in Fig. 5(a), in comparison to $MAPbI_3$ and $MAPbBr_3$ (see Fig. 6). Therefore, these results confirm our experimental findings obtained by optical spectroscopy that possible crystal phase transitions are suppressed in the Cs0.05 perovskite for temperatures up to room temperature.

In summary, we have demonstrated the suppression of possible phase transitions in Cs-containing multiple-cation mixed-halide perovskites for temperatures T = 10–300 K by combining temperature-dependent absorption and electroreflectance spectroscopy as well as X-ray diffraction. Moreover, we determined the exciton binding energy E_B of these compounds directly by a careful and detailed evaluation utilizing generalized Elliott fits and, additionally, by the so-called f-sum method. The obtained values for these compounds are even below the results for pure $MAPbI_3$ emphasizing their suitability for photovoltaic applications due to improved charge-carrier separation and collection.

We acknowledge financial support by the German Federal Ministry of Education and Research (BMBF) under Project No. FKZ 03SF0516 and the Karlsruhe School of Optics and Photonics (KSOP) at KIT. M.F.A. gratefully acknowledges support by the Scientific and Technological Research Council of Turkey. We also acknowledge support by Deutsche Forschungsgemeinschaft and Open Access Publishing Fund of Karlsruhe Institute of Technology.

APPENDIX A: TEMPERATURE-DEPENDENT X-RAY DIFFRACTOGRAMS OF $MAPbI_3$ AND $MAPbBr_3$

Temperature-dependent X-ray diffraction patterns were obtained similar to the Cs0.05 compound (presented in Fig. 5) also for pure $MAPbI_3$ and $MAPbBr_3$. The resulting diffractogramms are summarized in Fig. 6 and exhibit clearly visible changes due to crystal phase transitions.

APPENDIX B: EXPERIMENTAL DETAILS

1. Electroreflectance spectroscopy

For the ER measurements, we used a 250 W halogen lamp followed by a 0.32 m focal-length monochromator with a 600 lines/mm grating for spectral filtering as tunable light source for the illumination of the sample. The reflected intensity R is recorded using a silicon photodetector connected to a Keithley multimeter. The sinusoidal AC bias [amplitude $V_{max} = \pm(0.5–1.0)$ V, $V_{DC} = 0$ V, frequency f = 990 Hz] for the modulation is provided by a function generator. The resulting change in reflection ΔR is measured using a lock-in amplifier. The detection can be realized at the fundamental frequency f or the second harmonic $2f$.

2. Temperature-dependent x-ray powder diffraction

To prepare the powder for the XRD measurements, perovskite films were fabricated as thin films on glass and scraped off the glass afterwards. The obtained sample was prepared with grease between two foils. Measurements were performed on a Huber

G670 Guinier Imaging Plate diffractometer with Co–$K_{\alpha 1}$ radiation (λ = 1.788965 Å) and a Ge (111) primary monochromator. The 2θ values of the obtained diffractograms were recalculated to the ones of Cu–$K_{\alpha 1}$ radiation in order to facilitate a direct comparison with other results. The diffractometer is equipped with a low-temperature device 670.4, a closed-cycle He cryostat (CTI-Cryogenics, model 22), and a temperature controller (Lakeshore, model 331) for temperature-dependent measurements in the range of 10–300 K.

REFERENCES

[1] S. De Wolf, J. Holovsky, S. J. Moon, P. Löper, B. Niesen, M. Ledinsky, F. J. Haug, J. H. Yum, and C. Ballif, "Organometallic halide perovskites: Sharp optical absorption edge and its relation to photovoltaic performance," J. Phys. Chem. Lett. **5**, 1035–1039 (2014).

[2] S. D. Stranks, G. E. Eperon, G. Grancini, C. Menelaou, M. J. P. Alcocer, T. Leijtens, L. M. Herz, A. Petrozza, and H. J. Snaith, "Electron-hole diffusion lengths exceeding 1 micrometer in an organometal trihalide perovskite absorber," Science **342**, 341–344 (2013).

[3] K. Handloser, N. Giesbrecht, T. Bein, P. Docampo, M. Handloser, and A. Hartschuh, "Contactless visualization of fast charge carrier diffusion in hybrid halide perovskite thin films," ACS Photonics **3**, 255–261 (2016).

[4] W. J. Yin, T. Shi, and Y. Yan, "Unusual defect physics in $CH_3NH_3PbI_3$ perovskite solar cell absorber," Appl. Phys. Lett. **104**, 063903 (2014).

[5] M. L. Petrus, J. Schlipf, C. Li, T. P. Gujar, N. Giesbrecht, P. Müller-Buschbaum, M. Thelakkat, T. Bein, S. Hüttner, and P. Docampo, "Capturing the sun: A review of the challenges and perspectives of perovskite solar cells," Adv. Energy Mater. **7**, 1700264 (2017).

[6] P. Docampo, J. M. Ball, M. Darwich, G. E. Eperon, and H. J. Snaith, "Efficient organometal trihalide perovskite planar-heterojunction solar cells on flexible polymer substrates," Nat. Commun. **4**, 2761 (2013).

[7] W. S. Yang, B.-W. Park, E. H. Jung, N. J. Jeon, Y. C. Kim, D. U. Lee, S. S. Shin, J. Seo, E. K. Kim, J. H. Noh, and S. I. Seok, "Iodide management in formamidinium-lead-halide based perovskite layers for efficient solar cells," Science **356**, 1376–1379 (2017).

[8] M. F. Aygüler, B. M. Puscher, Y. Tong, T. Bein, A. S. Urban, R. D. Costa, and P. Docampo, "Light-emitting electrochemical cells based on inorganic metal halide perovskite nanocrystals," J. Phys. D: Appl. Phys. **51**, 334001 (2018).

[9] F. Deschler, M. Price, S. Pathak, L. E. Klintberg, D. D. Jarausch, R. Higler, S. Hüttner, T. Leijtens, S. D. Stranks, H. J. Snaith, M. Atatüre, R. T. Phillips, and R. H. Friend, "High photoluminescence efficiency and optically pumped lasing in solution-processed mixed halide perovskite semiconductors," J. Phys. Chem. Lett. **5**, 1421–1426 (2014).

[10] P. Brenner, M. Stulz, D. Kapp, T. Abzieher, U. W. Paetzold, A. Quintilla, I. A. Howard, H. Kalt, and U. Lemmer, "Highly stable solution processed metal-halide perovskite lasers on nanoimprinted distributed feedback structures," Appl. Phys. Lett. **109**, 141106 (2016).

[11] C. M. Sutter-Fella, Y. Li, M. Amani, J. W. Ager, F. M. Toma, E. Yablonovitch, I. D. Sharp, and A. Javey, "High photoluminescence quantum yield in band gap tunable bromide containing mixed halide perovskites," Nano Lett. **16**, 800–806 (2016).

[12] D. P. McMeekin, G. Sadoughi, W. Rehman, G. E. Eperon, M. Saliba, M. T. Horantner, A. Haghighirad, N. Sakai, L. Korte, B. Rech, M. B. Johnston, L. M. Herz, and H. J. Snaith, "A mixed-cation lead mixed-halide perovskite absorber for tandem solar cells," Science **351**, 151–155 (2016).

[13] O. A. Syzgantseva, M. Saliba, M. Grätzel, and U. Rothlisberger, "Stabilization of the perovskite phase of formamidinium lead triiodide by methylammonium, Cs, and/or Rb doping," J. Phys. Chem. Lett. **8**, 1191–1196 (2017).

[14] M. Saliba, T. Matsui, J.-Y. Seo, K. Domanski, J.-P. Correa-Baena, M. K. Nazeeruddin, S. M. Zakeeruddin, W. Tress, A. Abate, A. Hagfeldt, and M. Grätzel, "Cesium-containing triple cation perovskite solar cells: Improved stability, reproducibility and high efficiency," Energy Environ. Sci. **9**, 1989–1997 (2016).

[15] National Renewable Research Laboratory, "NREL Efficiency Chart" (2019) http://www.nrel.gov/.

[16] R. J. Elliott, "Intensity of optical absorption by excitons," Phys. Rev. **108**, 1384–1389 (1957).

[17] M. Saba, M. Cadelano, D. Marongiu, F. Chen, V. Sarritzu, N. Sestu, C. Figus, M. Aresti, R. Piras, A. Geddo Lehmann, C. Cannas, A. Musinu, F. Quochi, A. Mura, and G. Bongiovanni, "Correlated electron-hole plasma in organometal perovskites," Nat. Commun. **5**, 5049 (2014).

[18] F. Ruf, A. Magin, M. Schultes, M. F. Aygüler, P. Docampo, E. Ahlswede, H. Kalt, and M. Hetterich, "Temperature-dependent electromodulation spectroscopy of excitons in perovskite solar cells," in *2018 IEEE 7th World Conference on Photovoltaic Energy Conversion (WCPEC), Waikoloa, HI, 2018*.

[19] N. Sestu, M. Cadelano, V. Sarritzu, F. Chen, D. Marongiu, R. Piras, M. Mainas, F. Quochi, M. Saba, A. Mura, and G. Bongiovanni, "Absorption f-sum rule for the exciton binding energy in methylammonium lead halide perovskites," J. Phys. Chem. Lett. **6**, 4566–4572 (2015).

[20] A. Miyata, A. Mitioglu, P. Plochocka, O. Portugall, J. T.-W. Wang, S. D. Stranks, H. J. Snaith, and R. J. Nicholas, "Direct measurement of the exciton binding energy and effective masses for charge carriers in organic-inorganic tri-halide perovskites," Nat. Phys. **11**, 582–587 (2015).

[21] K. Galkowski, A. Mitioglu, A. Miyata, P. Plochocka, O. Portugall, G. E. Eperon, J. T.-W. Wang, T. Stergiopoulos, S. D. Stranks, H. J. Snaith, and R. J. Nicholas, "Determination of the exciton binding energy and effective masses for methylammonium and formamidinium lead tri-halide perovskite semiconductors," Energy Environ. Sci. **9**, 962–970 (2016).

[22] V. D'Innocenzo, G. Grancini, M. J. P. Alcocer, A. R. S. Kandada, S. D. Stranks, M. M. Lee, G. Lanzani, H. J. Snaith, and A. Petrozza, "Excitons versus free charges in organo-lead tri-halide perovskites," Nat. Commun. **5**, 3586 (2014).

[23] T. J. C. Hosea, "Estimating critical point parameters of modulated reflectance spectra," Phys. Status Solidi B **189**, 531 (1995).

[24] A. Grau, T. Passow, and M. Hetterich, "Temperature dependence of the GaAsN conduction band structure," Appl. Phys. Lett. **89**, 202105 (2006).

[25] A. Poglitsch and D. Weber, "Dynamic disorder in methylammoniumtrihalogenoplumbates (II) observed by millimeter-wave spectroscopy," J. Chem. Phys. **87**, 6373 (1987).

[26] M. A. Green, Y. Jiang, A. M. Soufiani, and A. Ho-Baillie, "Optical properties of photovoltaic organic-inorganic lead halide perovskites," J. Phys. Chem. Lett. **6**, 4774–4785 (2015).

[27] F. Panzer, S. Baderschneider, T. P. Gujar, T. Unger, S. Bagnich, M. Jakoby, H. Bässler, S. Hüttner, J. Köhler, R. Moos, M. Thelakkat, R. Hildner, and A. Köhler, "Reversible laser induced amplified spontaneous emission from coexisting tetragonal and orthorhombic phases in hybrid lead halide perovskites," Adv. Opt. Mater. **4**, 917–928 (2016).

[28] M. I. Dar, G. Jacopin, S. Meloni, A. Mattoni, N. Arora, A. Boziki, S. M. Zakeeruddin, U. Rothlisberger, and M. Grätzel, "Origin of unusual bandgap shift and dual emission in organic-inorganic lead halide perovskites," Sci. Adv. **2**, e1601156 (2016).

[29] R. Prasanna, A. Gold-Parker, T. Leijtens, B. Conings, A. Babayigit, H. G. Boyen, M. F. Toney, and M. D. McGehee, "Band gap tuning via lattice contraction and octahedral tilting in perovskite materials for photovoltaics," J. Am. Chem. Soc. **139**, 11117–11124 (2017).

[30] B. O. Seraphin and N. Bottka, "Band-structure analysis from electro-reflectance studies," Phys. Rev. **145**, 628–636 (1966).

[31] D. E. Aspnes, "Third-derivative modulation spectroscopy with low-field electroreflectance," Surf. Sci. **37**, 418–442 (1973).

[32] C. Huber, C. Krämmer, D. Sperber, A. Magin, H. Kalt, and M. Hetterich, "Electroreflectance of thin-film solar cells: Simulation and experiment," Phys. Rev. B **92**, 75201 (2015).

[33] C. Krämmer, C. Huber, A. Redinger, D. Sperber, G. Rey, S. Siebentritt, H. Kalt, and M. Hetterich, "Diffuse electroreflectance of thin-film solar cells: Suppression of interference-related line shape distortions diffuse electroreflectance of thin-film solar cells: Suppression of interference-related line shape distortions," Appl. Phys. Lett. **107**, 222104 (2015).

[34]M. E. Ziffer, J. C. Mohammed, and D. S. Ginger, "Electroabsorption spectroscopy measurements of the exciton binding energy, electron-hole reduced effective mass, and band gap in the perovskite $CH_3NH_3PbI_3$," ACS Photonics **3**, 1060–1068 (2016).
[35]F. Ruf, A. Magin, M. Schultes, E. Ahlswede, H. Kalt, and M. Hetterich, "Excitonic nature of optical transitions in electroabsorption spectra of perovskite solar cells," Appl. Phys. Lett. **112**, 083902 (2018).
[36]Fluorine-doped Tin Oxide.
[37]2,2′,7,7′-tetrakis-(N,N-di-p-methoxyphenyl-amine)-9,9′-spirobifluorene .
[38]B. V. Shanabrook, O. J. Glembocki, and W. T. Beard, "Photoreflectance modulation mechanisms in GaAs-$Al_xGa_{1-x}As$ multiple quantum wells," Phys. Rev. B **35**, 2540–2543 (1987).
[39]F. H. Pollak and O. J. Glembocki, "Modulation spectroscopy of semiconductor microstructures: An overview," Proc. SPIE **0946**, 34 (1988).
[40]M. Galluppi, L. Geelhaar, H. Riechert, M. Hetterich, A. Grau, S. Birner, and W. Stolz, "Bound-to-bound and bound-to-free transitions in surface photovoltage spectra: Determination of the band offsets for $In_xGa_{1-x}As$ and $In_xGa_{1-x}As_{1-y}N_y$ quantum wells," Phys. Rev. B **72**, 1–12 (2005).
[41]J. E. Rowe and D. E. Aspnes, "Approximate treatment of exciton effects in electric field modulation via the Slater-Koster interaction," Phys. Rev. Lett. **25**, 162–165 (1970).
[42]M. Bouduban, A. Burgos-Caminal, and J. E. Moser, "Unveiling the nature of charge carrier interactions by electroabsorption spectroscopy: An illustration with lead-halide perovskites," CHIMIA **71**, 231–235 (2017).